Chinese Chemical Letters 33 (2022) 2316–2326

Contents lists available at ScienceDirect

Chinese Chemical Letters

journal homepage: www.elsevier.com/locate/cclet

Research progress of tunnel-type sodium manganese oxide cathodes for SIBs

Jie Feng[a,d], Shaohua Luo[a,b,c,d,e,*], Kexing Cai[a,d], Shengxue Yan[a,d], Qing Wang[a,c,d], Yahui Zhang[a,c,d], Xin Liu[a,c,d]

[a] School of Materials Science and Engineering, Northeastern University, Shenyang 110819, China
[b] State Key Laboratory of Rolling and Automation, Northeastern University, Shenyang 110819, China
[c] School of Resources and Materials, Northeastern University at Qinhuangdao, Qinhuangdao 066004, China
[d] Key Laboratory of Dielectric and Electrolyte Functional Material Hebei Province, Qinhuangdao 066004, China
[e] Qinhuangdao Laboratory of Resources Cleaner Conversion and Efficient Utilization, Qinhuangdao 066004, China

ARTICLE INFO

Article history:
Received 18 July 2021
Revised 20 August 2021
Accepted 23 September 2021
Available online 29 September 2021

Keywords:
Sodium-ion batteries
$Na_{0.44}MnO_2$
Cathode materials
Doping
Nonaqueous electrolytes

ABSTRACT

Among the large energy storage batteries, the sodium ion batteries (SIBs) are attracted huge interest due to the fact of its abundant raw materials and low cost, and has become the most promising secondary battery. Tunnel-type sodium manganese oxides (TMOs) are industrialized cathode materials because of their simple synthesis method and proficient electrochemical performance. $Na_{0.44}MnO_2$ (NMO) is considered the best candidate material for all tunnel-type structural materials. In this paper, the research progress in charge and discharge of cathode materials for tunnel-type structural SIBs is reviewed, the redox mechanism and all sorts of synthesis methods and different coating methods lead to different morphology and electrochemical properties of materials and the classification of electrolytes and nonaqueous electrolytes. The development and utility of aqueous solutions are discussed, and the mechanism is analyzed. Summarized the cationic potential of the transition metal oxide for tunnel structure, plays a vital role in predicting and designing the cathode material of this structure. In addition, the future opportunities and challenges for such tunnel-type SIBs in this field are described in detail.

1. Introduction

The depletion of fossil resources makes the development of large-scale energy storage systems facing challenges for researchers. At present, the development of cheap and efficient energy storage devices is the top priority for the widespread use of new energy devices. With the development of new energy vehicles and large-scale energy storage equipment, the demand for lithium resources is increasing, and the reserves of lithium resources are limited and unevenly distributed [1]. Therefore, it is necessary to find new energy sources to alleviate the current shortage of lithium resources. Due to the limited supply of lithium, people are progressively interested in batteries such as sodium ion, potassium ion [2], multivalent calcium ion [3], magnesium ion [4] and zinc ion [5]. The Na_xMnO_2 batteries have advantages in terms of cost, safety and performance. They have been extensively studied in SIBs and are sustainable [6–9]. Cathode materials are one of the important components of SIBs. They are mainly combined with manganese oxides [10], polyanionic compounds [11], Prussian blue analogs [12], Organic material [13] and different types [14] of large-scale energy storage. According to the stacking sequence of oxygen and the occupation position of sodium ions, layered cathode materials can be further divided into P2 and O3 phases, where P and O represent the coordination environment of Na^+ for prism and octahedron, respectively, and 2 and 3 represent the transition metal layers in the cycle unit. The stacking sequence of oxygen and the occupation position of sodium ions. Since most inorganic materials are derived from depleted mineral resources, their synthesis and deintercalation not only need to consume energy, but also generate numerous emissions. Due to the difficulty of recycling and utilization, organic materials have better redox stability, structural diversity and environmental friendliness. The application of SIBs in large-scale energy storage equipment is shown in Fig. 1a [15]. Doeff *et al.* proposed the method of inserting lithium into the orthogonal nano-MnO_2 material, and gave the electrochemical performance, thermal performance and structural characteristics of the material [16]. Fig. 1b shows the relationship between

* Corresponding author at: School of Resources and Materials, Northeastern University at Qinhuangdao, Qinhuangdao 066004, China.
E-mail address: tianyanglsh@163.com (S. Luo).

https://doi.org/10.1016/j.cclet.2021.09.077
1001-8417/

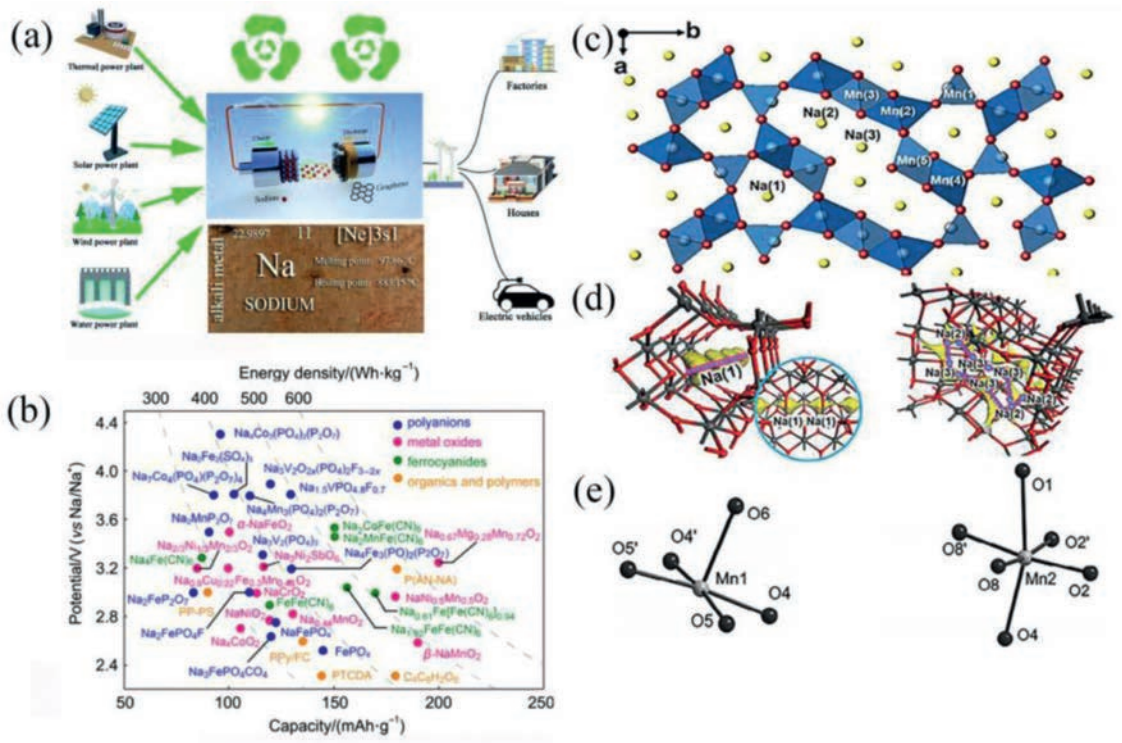

Fig. 1. (a) The way SIBs are used in large energy storage devices. (b) Relationship between energy density and discharge capacity. (c) Crystal structure of tunneled transition metal oxide NMO. Reproduced with permission [17]. Copyright 2021, Wiley-VCH. (d) Local magnification of the Na (1, 2, 3) diffusion location. Reproduced with permission [29]. Copyright 2020, Wiley-VCH. (e) Mn^{3+}-O coordination of the Mn1 site and Mn2 site. Reproduced with permission [25]. Copyright 2011, Wiley-VCH.

energy density and discharge capacity [17]. Parant *et al*. isolated many new ternary oxides manganese-oxygen-sodium system for Na/Mn $\leq$ 1, and proposed that they have two isomers. However, the electrochemical properties of diamond shaped Na_xMnO_2 have not been studied [18]. Mendiboure *et al*. used cyclic voltammetry method to measure NMO intercalation/deintercalation actions and submitted two types of Na^+ sites to explain NMO limited insertion ability [19]. Doeff *et al*. applied NMO to SIBs and proposed that the sodium storage site in Na_xMnO_2 has a small tunnel and four large s-shaped channels for the first time, as shown in Fig. 1c [20]. Sodium and lithium belong to the same main group, with little difference in electrochemical properties, rich sodium resources, low price, and non-toxicity. Sodium-ion batteries have become one of the batteries that are expected to alleviate the problem of blocked battery technology development caused by the lack of lithium resources. The working principle of SIBs are similar with lithium-ion batteries. It is also a concentration difference battery (also known as a "swing battery"). During the charging process, Na^+ is released from the positive electrode material and inserted into the negative electrode material through the electrolyte and the separator, thus the concentration difference between the positive and negative electrodes of the battery is generated, and electrical energy is converted into chemical energy. The discharge process is exactly the opposite [21,22]. Repeated charge and discharge processes to achieve energy storage and supply purposes [23].

The charging and discharging process of NMO is mainly the transition between NMO and MnO_2 phases (Eqs. 1 and 2). The charging and discharging process can be expressed by the following formula (Eqs. 1 and 2):

$$\text{Charging process: } Na_xMnO_2 - xNa^+ - xe^- \rightarrow MnO_2 \quad (1)$$

$$\text{Discharging process: } MnO_2 + xNa^+ + xe^- \rightarrow Na_xMnO_2 \quad (2)$$

During the charging process, the positive electrode is oxidized and Na^+ separates from NMO to form a MnO_2 phase. During the discharge process, the cathode is reduced, Na^+ is embedded in the cathode material, and the MnO_2 phase is transformed into NMO [24].

NMO has attracted the attention of researchers due to its unique crystal structure. Tunnel structure manganese-based cathode material NMO has entered the public view. This article first reviews the structure mechanism and ion kinetics of NMO, and summarizes the synthesis methods and modification methods of NMO synthesis, tunnel introduction of the latest results of NMO in aqueous and non-aqueous electrolyte solutions. The existing problems and possible solutions are discussed, and the prospect of large-scale industrial production of NMO is proposed in the end.

2. Structural mechanism and dynamics

2.1. Structure mechanism

NMO is a contractual structure of $Na_4Mn_9O_{18}$ and has an orthorhombic lattice structure. MnO_5 quadrangular pyramid and MnO_6 octahedron constitute the entire unit cell structure. At the same time, Mn ions are distributed in different regions. All Mn^{4+} ions and half of the Mn^{3+} ions are located at the octahedral site of MnO_6, and Mn^{3+} are located at the position of the MnO_5 square pyramid within the lattice [25]. The tetrahedron connects two octahedral chains shared by two sides and one three sides, forming a large S-shaped tunnel stabilized by four rows of Na^+ and a smaller tunnel stabilized by one sodium ion [26–28]. A tunnel channel can maintain a smooth position in the channel through a discontinuous polygon tunnel, and the channel does not meet the requirements of Na(1) and Na(2) in Fig. 1d [29], the position in the *S*-shape. The Mn particle within the structure has Mn^{3+} and Mn^{4+} cornice domain that area unit charge-neutral, given as

$Na_4^{1+}Mn_4^{3+}Mn_5^{4+}O_{18}^{2-}$. NMO monocrystals were synthesized by the flow method in 1173 K for the first time. The characteristic Mn^{3+}-O coordination for the Mn1 and Mn2 sites in the present NMO structure are shown in Fig. 1e [25]. Na^+ tend to move toward the center in the *S*-type tunnel. The Jahn-Teller distortion can be determined by the key distance variance. The Jahn-Teller effect describes the instability of a nonlinear molecular system in a degenerate electron state, which eliminates degeneracy and forms a new system with low symmetry and low energy. In the nonlinear MnO_6 octahedral field, Mn^{3+} generally exists in a high spin state and has a very large magnetic moment, which causes the linear MnO_2 arrangement to elongate along the axial direction, resulting in Jahn-Teller distortion. The high spin Mn^{3+} ion has only one electron in the doubly degenerate e_g orbital, which leads to the asymmetry of its electron distribution, and the electrons in the end orbital show different shielding effects on Mn nucleus in different directions. To stabilize the Mn^{3+} ion, the two longitudinal Mn-O bonds will be elongated and the four horizontal Mn-O bonds will be shortened. Therefore, the dramatic structural changes caused by the Jahn-Teller effect caused by high spin Mn^{3+} ions seriously affect the electrochemical cycling performance for NMO materials. The transformation of high spin Mn^{3+} ions into low spin states will also expecting suppress the Jahn-Teller effect. The content percentage of Mn^{4+} and Mn^{3+} can also be determined by the diversity of Mn sites. It provides a way to understand the relative charge of the Mn site. Kruk *et al.* [30] reported the relationship between the share of manganese sites associated with sodium sites. The discrimination spectrum of $Na_{0.4}(2)$-MnO_2 was obtained by Rietveld analysis of the optical phenomenon information of X-ray synchrotron. From the analysis of soft X-ray absorption spectroscopy (sXAS), the process of absorbing incident photons may lead to the release of electrons from the atomic nucleus of the vacancy state in the left panel. In principle, after the central electron is excited by collision, the excited state shows various characteristics. Otherwise, under the influence of intermediate holes, the shell electrons are excited, vibrated and rotated, and the charge is excited. After the last shell electron is excited and attenuated, as shown in Fig. S1 (Supporting information).

2.2. Ion dynamics

High structural stability is one of the most prominent advantages of sodium manganese oxide tunnel-type structure. Baudrin *et al.* first proposed a mechanism for medium storage of sodium in 2007 [27]. The combination of potentiostat intermittent titration technique and *in situ* X-ray diffraction measurement can prove that there were six two-phase transitions in the set voltage range (relative to Na^+/Na). The insertion process was completely reversible in the composition range $0.25 < x < 0.65$ and provides a certain degree of irreversibility when x was less than 0.25. More detailed mechanisms were studied by combining electrochemical characterization, such as cyclic voltammetry, structural determination, infrared spectroscopy and thermal barrier calculation. Chae *et al.* [29] showed that the diffusion barrier of Na(1) site was significantly higher than that of Na(2) and Na(3) sites. The reason for the faster diffusion of sodium ions in NMO structure is that the activation barrier of three sodium sites is weaker than that of other sites. The redox state of manganese atom can be determined by the distance between particles. Due to the relatively small attraction of manganese bonds, the length of Mn-O increases slightly from 1.906 Ω to 1.980 Ω with slight Jahn-Teller distortion.

The chemical diffusion coefficient of Na^+ was improved by the Intermittent Galvanostatic Titration Technique test and by the Electrochemical Impedance Spectroscopy test. The yield of the electrodes depends on the density of the active Na^+ transport planes (d), the solid phase diffusion in the electrode (D) and on the diffusion length (L). That is Eq. 3 [31]:

$$\text{Kinetics } \alpha \sim \frac{D}{L^2} d \tag{3}$$

The geometric diffusion parameters of the materials (L) and the density of the active transmission planes (d) can be vital for the velocity characteristics of the materials. As the depth of sodium removal increases, the charge transfer resistance first decreases and then increases, and the diffusion coefficient of Na^+ in solid materials first increases and then decreases. As the number of cycles increases, the charge transfer resistance of the material increases, the diffusion coefficient of Na^+ in the material decreases, and the electrochemical performance of the material deteriorates. From a crystallographic point of view, the diffusion path of Na^+ through the Na(2) and Na(3) positions is more accessible to identify than the Na(1) position. Therefore, at the Na(1) position, Na^+ operate by a hopping mechanism at this position, and at the Na(2) and Na(3) positions, Na^+ operate through diffusion this position. The Na^+ at the Na(2) and Na(3) positions have triangular prism coordination with the Na-O bond at a distance of 2.3–2.4 Å During the intercalation/deintercalation, Na^+ are transmitted along the *c*-axis in the specified direction.

The solid line part of the sXAS spectrum at the edge of Mn-L shows that Mn^{2+} collected on the electrode, Mn^{3+} and Mn^{4+} are in the initial charge ($Na_{0.22}MnO_2$, 1Ch) and initial discharge ($Na_{0.66}MnO_2$, 1D). The dotted line is the calculated spectrum of the electrode sample. The spectrum was a linear combination of three reference spectra, which can directly measure Mn^{2+}, Mn^{3+} and Mn^{4+} [32]. Also, the sXAS of the NMO electrode were studied comprehensively. A comparison diagram of the collected experimental data and calculated experimental data with solid lines and dashed lines under different electrochemical potentials. A graph showing the relationship between manganese ion concentration and sodium ion concentration of different valence states in the electrode during the reflection process [33], as shown in Fig. S2 (Supporting information).

The special *quasi*-random structure (SQS) methodology is applied to mimic the disordered NMO, and supported this, the simulation of molecular dynamics and the calculations of the primary principle are used to study the Na^+ diffusion mechanism and the transport pathways after reasonable approximations [34]. The best adjustable equivalent circuits were shown within the part of Figs. 2a and b. To look at the diffusion mechanism obtained by molecular dynamics (MD), the bond valence-energy state-landscape mapping (BVEL) was shown in Fig. 2c. In the part of Figs. 2d–h [34], all possible trajectories of the minimum energy paths (MEPs) between two ions along the axial direction are shown. The graph shows the energy distribution of the two ions in the migration process. Fig. 3 clearly shows the structural changes of Na^+ during intercalation and deintercalation. The 2D *in-situ* XRD patterns and charge-discharge curves of the first three cycles and the XRD patterns of Ti (004) peak after the first three cycles are shown in Fig. 3a. Fig. 3b shows the XRD patterns of peak T2 (102) (200), the lattice parameters of *a*-axis and *c*-axis T1 structure, the lattice parameters of P2 structures *A* and *C*, and the lattice parameters of *a* and *c* in T2 system. Fig. 3c shows the volume changes of T1 structure, P2 structure and T2 structure in three periods [35].

In recent years, the research of tunnel manganese oxides has made extensive progress. The specific capacity synthesis methods, electrochemical properties and voltage range of tunnel-type manganese oxides are summarized in this paper of Table 1.

Zhao *et al.* [36] first reported the cationic potential to calculate the interaction between cathode materials, which could be used to predict the stacking structure (Eq. 4). They define the cationic potential to indicate the electron density and polarization of the

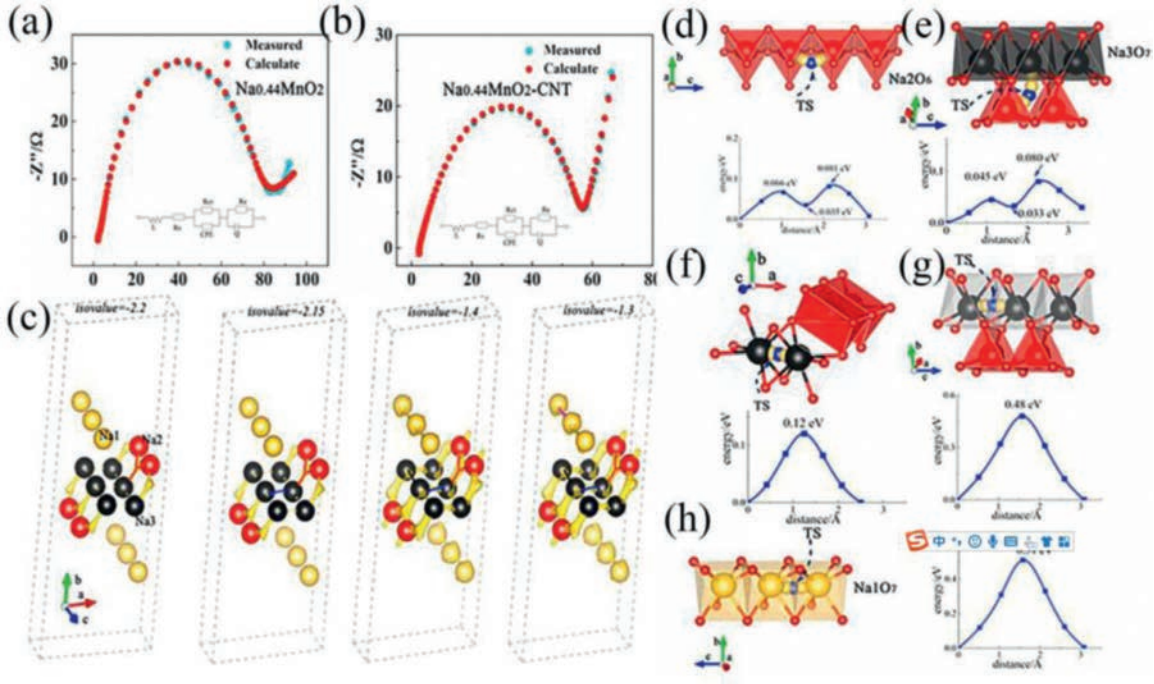

Fig. 2. (a) Patterns of NMO. (b) Patterns of $Na_{0.44}MnO_2$-CNT, and the equivalent circuit diagram at the bottom of the figure is the equivalent circuit when the simulated temperature is about 1200 K. (c) The red line shows the diffusion between two Na(2)-Na(2) atoms and Na(2)-Na(3) atoms, The blue line represents the diffusion relationship between two Na3 atoms, The thick black line shows the diffusion of Na3 along the *c* axis, The purple line represents the diffusion of Na1 along the *c* axis. Energy distributions along with the MEP between. (d) Na(2) and Na(3) ions. (e) Na(3) and Na(3) ions along *b*-axis. (f) Na(3) and Na(3) ions along *a*-axis. (g) Na(3) and Na(3) ions along the *c*-axis. (h) Na(1) and Na(1) ions along the *c*-axis. Reproduced with permission [34]. Copyright 2021, Elsevier Ltd.

Table 1
Review of tunnel-type manganese oxides in nonaqueous SIBs.

Synthesis material	Voltage range	Electrolyte	Rev. capacity	Refs.
NMO (polymer-pyrolysis)	2.0–4.0 V	1 mol/L $NaClO_4$ EC/DMC	84.2/1000th/0.5 C	[60]
NMO (electrospun)	1.5–4.0 V	1 mol/L $NaClO_4$ EC/DMC	60/100th/50 mA/g	[61]
NMO (electrospun)	2.0–4.0 V	1 mol/L $NaClO_4$ PC/FE	117.2/200th/0.1 C	[62]
NMO (reverse microemulsion)	2.0–3.8 V	1 mol/L $NaClO_4$ PC	80.2/50th/100 mA/g	[64]
NMO (urea-combustion)	2.0–4.0 V	1 mol/L $NaClO_4$ PC/FEC	130/300th/4 C	[86]
NMO (spray pyrolysis)	2.0–4.0 V	1 mol/L $NaClO_4$ EC/DEC/ FEC	82/200th/1000 mA/g	[65]
NMO (solid-state)	2.0–3.8 V	1 mol/L $NaPF_6$	88.2/30th/1 C	[81]
NMO (PVP-combustion)	2.0–3.46 V	1 mol/L $NaClO_4$ PC	108/100th/1 C	[33]
NMO (PVP-combustion)	2.0–4.0 V	1 mol/L $NaClO_4$ PC	120/2nd/0.2 C	[63]
NMO (sol-gel)	2.0–4.0 V	1 mol/L $NaClO_4$ EC/DC	62/100th/11.1 mA/g	[58]
NMO (sol-gel)	2.0–4.0 V	1 mol/L $NaClO_4$ PC/EC	105/100th/0.1 C	[87]
NMO (sol-gel)	2.0–4.0 V	1 mol/L $NaClO_4$ EC/DEC	40/50th/0.1 C	[91]
NMO (sol-gel)	2.0–4.2 V	1 mol/L $NaClO_4$ PC/EC	41/500th/20 C	[39]
NMO (ultrasonic sonochemical)	2.0–4.0 V	1 mol/L $NaClO_4$ EC/PC	52/130th/1 C	[71]
$Na_{0.66}[Mn_{0.66}Ti_{0.34}]O_2$(solid state)	2.5–3.9 V	1 mol/L $NaClO_4$ EC/DEC	122/300th/3 C	[37]
$Na_{0.44}Ti_{0.33}Mn_{0.67}O_2$ (solid state)	1.8–2.8 V	1 mol/L $NaClO_4$ DEC/EC	105/100th/0.1 C	[38]
$Na_{0.44}Mn_{0.89}Co_{0.11}O_2$ (thermopolymerization)	2.0–4.0 V	1 mol/L $NaClO_4$ DEC/EC/ FEC	166/40th/12 mA/g	[101]
$Na_{0.44}Mn_{2/3}Co_{1/6}Ni_{1/6}O_2$ (thermopolymerization)	2.0–4.0 V	1 mol/L $NaClO_4$ EC/DC	118/100th/1 C	[72]
$Na_{0.44}Mn_{0.95}Mg_{0.05}O_2$ (solid-state)	2.0–3.8 V	1 mol/L $NaClO_4$ EC/PC	59/800th/2 C	[103]
$Na_{0.61}[Mn_{0.27}Fe_{0.34}Ti_{0.39}]O_2$ (solid-state)	3.4–4.2 V	0.8 mol/L $NaPF_6$ PC	99/100th/0.2 C	[43]
$Na_{0.44}MnO_{1.93}F_{0.07}$ (oxalate precursor)	2.0–4.2 V	1 mol/L $NaClO_4$ EC/PC/FEC	109/400th/5 C	[102]
$Na_{0.44}Mn_{0.98}Zr_{0.02}O_2$ (oxalate precursor)	2.0–4.0 V	1 mol/L $NaClO_4$ PC/EC/ FEC	89/500th/1 C	[73]
$Na_{0.61}Ti_{0.48}Mn_{0.52}O_2$ (solid-state)	1.5–4.7 V	1 mol/L $NaPF_6$ EC/DEC	70/100th/0.2 C	[96]
$Na_{0.44}MnO_{1.93}F_{0.07}$ (coprecipitation)	2.0–4.1 V	1 mol/L $NaClO_4$ EC/PC	137.5/100th/0.5 C	[67]
$Na_{0.6}MnO_2$-CTAB (coprecipitation)	2.0–4.0 V	1 mol/L $NaClO_4$ PC	130/70th/0.1 C	[68]
NMO@CNT (hydrothermal)	2.5–3.5 V	1 mol/L $LiPF_6$ EC/DC	147/50th/0.1 mA/g	[50]
NMO@graphene (hydrothermal)	2.0–4.0 V	1 mol/L $NaClO_4$ PC/EC	91.8/100th/50 mA/g	[57]
NMO@rGO (sol-gel)	2.0–4.0 V	1 mol/L $NaClO_4$ DEC/EC	124/200th/0.2 C	[93]
NMO@Al_2O_3 (solid-state)	2.0–4.5 V	1 mol/L $NaClO_4$ PC/EC	109.8/200th/0.4 C	[45]
NMO@Mn_2MoO_4 (solid-state)	1.5–4.3 V	0.5 mol/L $NaPF_6$ PC/FEC	103.2/200th/0.1 C	[107]

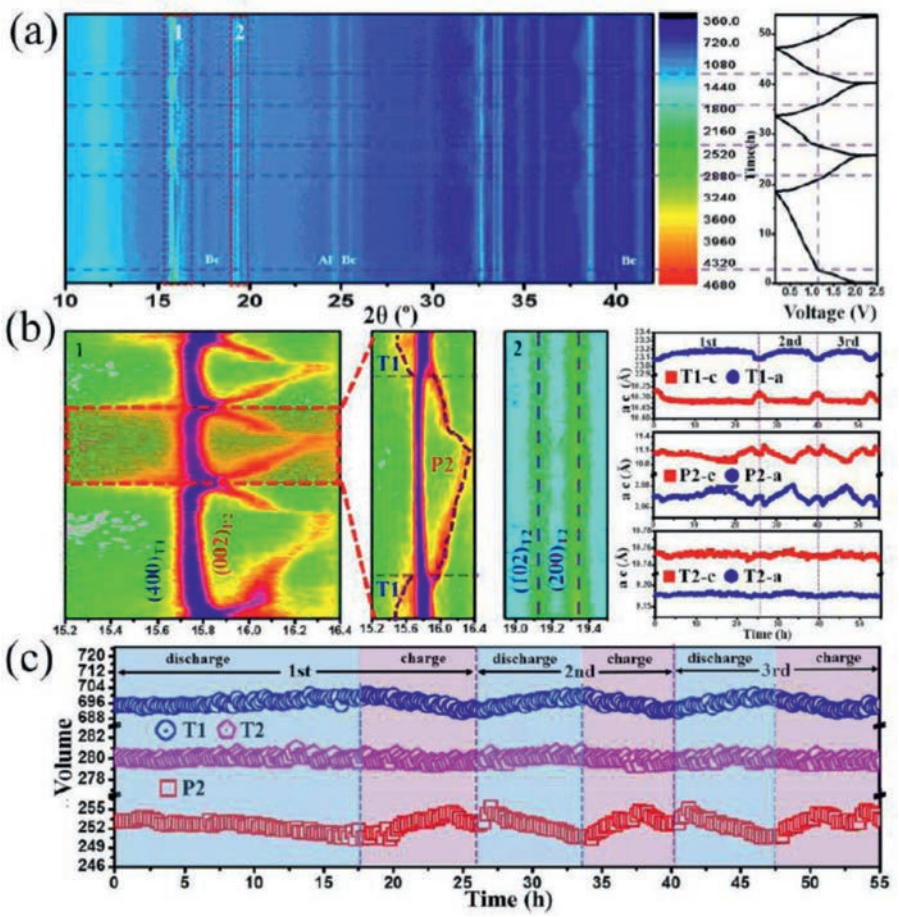

Fig. 3. (a) 2D *in-situ* EXRD patterns of charge/discharge curves in the first three cycles. (b) The T1 and P2 peaks of XRD patterns at the first and the second cycle, and T2 peaks of XRD patterns, Lattice parameter for T1, P2, and T2 of *a* and *c* axes. (c) Volumetric change for T1, P2 and T2 structure. Reproduced with permission [35]. Copyright 2018, Elsevier Ltd.

cationic, by defining the "cationic potential":

$$\emptyset_{\text{cation}} = \frac{\overline{\emptyset_{\text{TM}}\emptyset_{\text{Na}}}}{\overline{\emptyset_{\text{o}}}} \quad (4)$$

The above equation shows the relation between the cationic potential $\emptyset_{\text{cation}}$ and the weighted average Na ionic potential $\overline{\emptyset_{\text{Na}}}$. Ion potential is an index that characterizes the surface charge density of ions and reflects the polarization power of cations. The ion potential increases with the oxidation state and atomic mass. Larger cation potential means stronger transition metal (TM) electron cloud extension and interlayer electrostatic repulsion, resulting in P2-type structure, with more covalent TM-O bonds and increased *d*(O-Na-O) distance. On the contrary, the larger average Na^+ potential obtained by increasing the Na content increases the shielding of the electrostatic repulsion between the TMO_2 sheets, which is beneficial to the O3 type structure. Considering the different Na content, oxidation states of TMs, the composition of TMs, the cationic potential of Na, TMs and oxygen and the ratio of total TMs are summarized in Table 2.

Table 2
The cationic potential of Na, TMs and oxygen and the ratio of total TMs, Na to oxygen.

Oxide	$\frac{\overline{\emptyset_{\text{TM}}\emptyset_{\text{Na}}}}{\emptyset_{\text{anion}}}$	$\overline{\emptyset_{\text{Na}}}$	$\overline{\emptyset_{\text{TM}}}$	$\overline{\emptyset_{\text{anion}}}$	Refs.
$Na_{0.44}MnO_2$	9.7827	4.3137	63.8876	28.1714	[71]
$Na_{0.66}[Mn_{0.66}Ti_{0.34}]O_2$	12.2941	6.4705	53.5025	28.1714	[37]
$Na_{0.44}Ti_{0.33}Mn_{0.67}O_2$	18.8869	4.3142	123.3333	28.1714	[38]
$Na_{0.44}Mn_{0.89}Co_{0.11}O_2$	9.5734	4.3142	62.5174	28.1714	[101]
$Na_{0.44}Mn_{2/3}Co_{1/6}Ni_{1/6}O_2$	8.6808	4.3142	56.6855	28.1714	[69]
$Na_{0.44}Mn_{0.95}Mg_{0.05}O_2$	3.3885	4.3142	26.0926	28.1714	[103]
$Na_{0.61}[Mn_{0.27}Fe_{0.34}Ti_{0.39}]O_2$	7.9310	4.3142	51.7894	28.1714	[104]
$Na_{0.44}Mn_{0.98}Zr_{0.02}O_2$	7.1079	4.3142	46.4146	28.1714	[73]
$Na_{0.61}Ti_{0.48}Mn_{0.52}O_2$	11.6760	5.8824	55.9215	28.1714	[96]

3. Host material research

Although Na_xMnO_2 as a cathode material for SIBs has the benefits of high theoretical capability, low toxicity, low cost, simple preparation process, due to the existence of trivalent manganese ions, the Jahn-Teller is prone to occur during charging and discharging, which leads to the crystal structure of the material. Changes were made that affected the electrochemical performance of Na_xMnO_2 electrode materials. At present, the strategies to enhance the electrochemical performance of Na_xMnO_2 chiefly embrace metal ion doping, nano-particles and surface coating. There will be explained in detail below.

3.1. Synthesis

Most of the research on sodium ion battery materials is carried the basis of the research on lithium-ion battery materials. Therefore, its synthesis method also draws on the synthesis method of lithium ions battery materials. The synthesis method of Na_xMnO_2 is similar with Li_xMnO_2. Various artificial techniques for preparation of NMO were according as well as solid-state [34,37–45], molten salt [46–49], hydrothermal [41,50–54], microwave [55], sol-

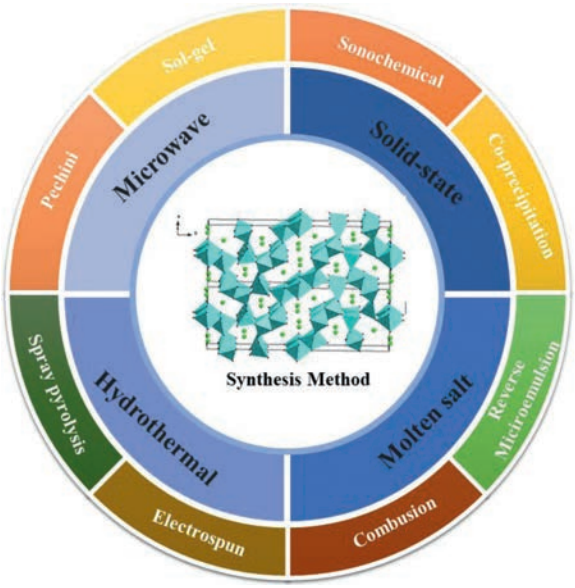

Fig. 4. Summary diagram of the composition method for NMO.

gel [56–58], spray pyrolysis [59], polymer-pyrolysis [60], electrospinning [61,62], combustion [63], reverse microemulsion [64–66], coprecipitation [67–69], glycine nitrate method [70], sonochemical methods [71] and other methods [72,73] are summarized in Fig. 4.

The high-temperature solid phase method is one of the commonly used methods in the synthesis of inorganic materials. This method has the advantages of simple operation process, easy control of reaction conditions, and low production cost. Therefore, it is widely used in the synthesis of various inorganic materials in industrial production. However, the disadvantages of this method are uneven composition, easy agglomeration of particles and wide distribution of particle diameter. The synthesis of Na_xMnO_2 by the high-temperature solid phase method is mainly to mix the sodium source and the manganese source uniformly according to a certain stoichiometric ratio, and the mixture undergoes a chemical reaction under high temperature conditions. Sodium-to-manganese ratio, roasting temperature and roasting time have a certain influence on the deintercalation process of Na^+ in the material. With the increase of sodium-to-manganese ratio, roasting temperature and roasting time, the solid electrolyte interphase (SEI) film diffusion activation energy W and interface of the synthesized material both the electrochemical reaction activation energy ΔG and the solid phase diffusion activation energy *Ea* show a trend of first decreasing and then increasing. Among them, the ratio of sodium to manganese has a small effect on the activation energy *F* of the diffusion of the synthetic material SEI membrane, and has a greater effect on the activation energy E_a of sodium ion diffusion in the solid phase, while the baking temperature and baking time have a greater effect on the activation energy E_a of sodium ion diffusion in the solid phase. The sol-gel method and the molten salt method can overcome this shortcoming, because the advantages of this method include the small particle size of the synthesized cathode material, the size can be from nanometer to micron, and the shape can be silk, thin and spherical, thus improving the performance. There are also some problems with sol-gel method, the raw materials used are expensive, some are organic, harmful to health, the reaction takes a long time, and many gasses and organic compounds will overflow during the drying process. Microwave is the electromagnetic wave between 300 MHz and 300 GHz. Its advantages are non-direct heating in order to avoid overheating on the surface of the material. It can be applied to various heating equipment such as domestic microwave ovens. But the amounts of materials synthesized by microwave method is small, and the instrument is more expensive than other methods. The advantages of electrospinning are simple and easy to operate. However, it is difficult to separate nanofibers from each other by electrospinning, and the current production of electrospinning machines is very low. When burning organic matter, it releases a lot of heat to reduce the final burning temperature. At the same time, when burning organic matter, it produces a lot of gas to reduce the agglomeration of products and the smaller particles of products. The products synthesized by this method have uniform particle size and composition, and the low sample synthesis temperature reduces the energy consumption. However, this method has small treatment amount and increases the cost after adding organic substances. For example, nanometer particles with higher crystallinity have better performance, and cathode materials that are intercalation/deintercalation along a given direction have relatively better performance [74]. The prepared electrode has good electrochemical performance. After 50 mA/g cycles in the range of 3.5–4.25 V, the initial discharge capacity is 145.5 mAh/g, and the capacity retention rate is 86.1%. After 50 cycles of 3.5–4.5 V, the discharge capacity reached 177.9 mAh/g, and the capacity retention rate was 85.6%. Zhou *et al.* had synthesized the Na_xMnO_2 ($x = 0.66$) three-dimensional tunnel-type cathode materials by chemical pretreatment with sodium biphenyl reagent. The initial charge capacity of cathode material obtained by this method is excellent [75]. In addition, increasing the surface area and shortening the diffusion length make the application of nanoparticles in rechargeable batteries very attractive. One of the foremost effective ways to boost power density is to reduce the cathode particles as much as possible. The nanoscale powder is calcined at 600 °C for six hours and then washed with a large quantity of water to get rid of impurities. Under the same cycle conditions, the capacity of the cathode material obtained is increased to 100 mAh/g. When cathode material is the nanoscale influence of anisotropic characteristics of the electronic structure, this can be achieved by electron energy loss spectroscopy (EELS) to prove that the spectra can be revealing the reduction of element valence state near electrode and metal oxide layer stack direction, which can reveal the cathode material anisotropy and explain the advantage of nanometer size to improve the electrochemical performance [76–78]. When the particle morphology is needle-like or rod-like, the cycling performance of the cathode material is better. This special morphology is characterized by a large surface area and volume, and it can still show good cycling performance when larger discharge current is generated. Excess sodium content plays a vital role in the formation of nanorods, which grow perpendicular to the grain direction. Due to the release of energy by Na^+ of deintercalation, the current and voltage characteristics of the battery formed by nanorods show six voltage platforms. Many mathematical models can be used to simulate and fit experimental data in NMO, which is thermodynamically consistent with the characteristics of a simple system [52,79–81].

The hydrothermal method is one of the commonly used methods for synthesize materials in the liquid phase method. The principle is that the reactants are placed in a high temperature and high-pressure kettle and the raw materials are synthesized by using water or other solvents as the medium. The material synthesized by hydrothermal method has high purity, uniform particle size and excellent crystallinity. The morphology of the product can be controlled by controling the reaction conditions. Hydrothermal method requires high equipment, technical and safety performance. The hydrothermal synthesis of Na_xMnO_2 is mainly based on the soluble sodium salt and manganese metal oxides as raw materials, with water or other solvents as the medium, in the reaction kettle for chemical reaction.

Su *et al*. synthesized $Na_{0.7}MnO_2$ nanosheets by hydrothermal method with a current density of 40 mA/g and a specific capacitance of 163 mAh/g, showing good electrochemical performance [82]. Liu *et al*. have synthesized Na-Mn-O composite materials by hydrothermal method. Using manganese sulfate and manganese nitrate as raw materials and H_2O_2 as oxidant, the metal oxide of manganese was prepared by electrodeposition method as a precursor, and then the precursor hydrothermal reaction took place with sodium hydroxide. After heat treatment, the reaction product was prepared with sodium manganese oxide composite material. At the current test density of 0.1 C, the first specific discharge capacity of the synthesized material is 185 mAh/g, which shows good electrochemical performance [83]. Tan *et al*. used the hydrothermal method to take Mn_2O_3 and NaOH as raw materials. The raw materials were placed in an autoclave and reacted for 46 to 96 h at 205 °C. After the reaction products were filtered, washed and dried, they were calcined at 600 °C for two hours, finally obtaining Na_xMnO_2 cathode materials [84]. Hosono *et al*. synthesized NMO cathode material by hydrothermal method using manganese tetroxide and sodium hydroxide as raw materials, first, 0.1 g of manganese tetroxide powder was weighed and dispersed in 50 mL of sodium hydroxide solution, then the solution was transferred to an autoclave for 96 h reaction at 205 °C, and the final product was filtered and washed and dried in vacuum at room temperature. The specific discharge capacity of the composite material was 115 mAh/g at the current test density of 0.42 C, and the capacity retention rate was 88% after 20 cycles at the current test density of 8.3 C [53]. Liu *et al*. synthesized NMO nanorods using $KMnO_4$, $MnSO_4$ and NaOH as raw materials by hydrothermal method, and investigated the effect of adding carbon nanotubes on the electrochemical properties of the materials. With the addition of carbon nanotubes, the material was tested at a test current density of 0.1 A/g. After 50 cycles, the capacity retention rate of the material increased from 70 °C to 82%, and the specific discharge capacity of the material increased from 45 to 99 mAh/g at a test current density of 2 A/g. The results show that the addition of carbon nanotubes is beneficial to improve the cyclic stability and rate performance of the materials [50]. Li *et al*. synthesized nanowire NMO by hydrothermal method. The Mn_2O_3 powder was dispersed in NaOH aqueous solution and reacted in a 200 °C reactor for two days. After centrifugation and washing, the reaction product was reacted with the same NaOH solution in a 200 °C reactor for two days. The final product was obtained by calcination at 600 °C for two hours. SEM results showed that the product was nanowire structure less than 100 nm [85].

To improve the performance of the cathode material, later in the research process, the method widely recognized by researchers is to shorten the ion diffusion length and expand the area of the electrode and electrolyte contact surface [41], synthesized nanoscale materials, various shapes such as stick [62,86–88], tablet [89], powder [59,90], super long submicron flat shape [91], nanofibers [65], polygon [61], nanowires [53,79,92], which further increases the interface charge dynamics, improving the electrochemical performance of sodium-ion intercalated. Liu *et al*. reported nanowires through electrospinning, and the process of synthesizing nanowires. The preparation of composite electrode can improve electronic conductivity. Liu *et al*. reported a NMO nanorod@CNA, the cyclic properties of the final composite material [53], which was a comparison of the cyclic performance of the composite electrode and the pure electrode at 0.1 A/g after 50 cycles. The discharge capacity of the composite electrode is about 4% higher than that of the pure electrode. Through comparison, the capacity retention rate of the pure electrode was much lower than that of the composite electrode, which was about 82% and 70%, respectively. NMO@rGO nanocomposite was prepared by using highly conductive reduced graphene oxide (rGO) by Fu *et al*. [93]. Due to the greatly increased ionic and electronic performance, and its electrochemical performance was significantly enhanced to 124 mAh/g at 0.2 C. PVP combustion synthesis technology has the best electrochemical performance among many synthesis methods. Through X-ray diffraction, scanning electron microscopy and high-resolution transmission electron microscopy to analyze its morphology and structure, all samples show good magnification ability, and the performance of the synthesized sample at 900 °C was the best discharge capacity 122.9 mAh/g at 5 C [63].

In addition to the above methods, there are also combustion and spray pyrolysis methods for the synthesis of NMO cathode materials. The principle of combustion method is that the polymer is pyrolyzed at high temperature. According to the experimental process, combustion method is also a sol-gel method. The difference is that the polymer releases a large amount of gas at high temperature, thereby inhibiting the growth of particle size of the material. Ferrara *et al*. [94] used combustion method to synthesize NMO cathode materials. Manganese nitrate tetrahydrate, sodium nitrate and urea were used as raw materials. The raw materials were dissolved in deionized water at a stoichiometry of 80 °C under continuous stirring condition. The final product was obtained by heat treatment from 500 °C to 700 °C for 2 h. At the test current density of 2 C and 5 C, the specific discharge capacity of the synthesized material was 95 mAh/g and 78 mAh/g, respectively. After 200 cycles, the capacity retention rate of the synthesized material was still 75.7%. Bucher *et al*. [95] synthesized sodium manganese oxide cathode materials by combustion method. With sodium nitrate and manganese acetate as raw materials, they were dissolved in deionized water at a certain stoichiometric ratio to form a solution. Then concentrated nitric acid and a small amount of gelatin were added to the solution, and the precursor powder was obtained by spontaneous combustion of the solution at 205 °C. The precursor was heat treated at 800 C for 4 h to obtain Na-Mn oxide cathode material. The specific discharge capacity of the synthesized material is 138 mAh/g at the test current density of 0.3 C, and 75 mAh/g after 20 cycles. Dai *et al*. [63] used $NaHCO_3$ and $Mn(OAc)_2{\cdot}4H_2O$ as raw materials and polyethylpyrrolidone as chelating agent to prepare NMO cathode material by gel-combustion method. The electrochemical performance of the synthesized material was tested in the voltage range of 2.4 V. The specific discharge capacity of the material was 122.9 mAh/g at the test current density of 0.2 C. It shows a high discharge specific capacity. Spray pyrolysis method is to dissolve the raw material in the solvent, and quickly evaporate the solvent in the solution with the spray device to get new solid particles. The particle size and morphology of the synthesized material are relatively uniform.

3.2. Cationic and anion substitution

The slow intercalation/deintercalation of sodium ions in tunnel-type SIBs and the slow transmission of sodium ions in the matrix material framework will greatly reduce the specific capacity and rate performance. The volume expansion caused by sodium ion implantation also causes the phase transformation and lattice change of the matrix material, making it difficult to obtain a good electrochemical stability. In addition, due to the low potential of sodium and large atomic mass, the specific energy of sodium ion battery is also lower than that of lithium-ion battery. So, building a cheap sodium-based material with high specific energy remains a challenge, mainly to overcome the low energy density and poor cycle life of SIBs. The theoretical capacity of NMO is about 120 mAh/g, and the capacity retention of NMO varies from hundreds of cycles to dozens of cycles, so there is a great space for improving the performance of tunneling materials. To improve the electrochemical performance of the cathode material, the researchers attempted to replace the manganese site of the NMO

cathode with anions [37,38,94,96]. The manganese site can be replaced by titanium ions without affecting the crystal structure, which can prevent the structural changes of Na^+ during intercalation/deintercalation. The cathode materials $Na_{0.44}Mn_{0.78}Ti_{0.22}O_2$ and $Na_{0.44}Mn_{0.67}Ti_{0.33}O_2$ have similar cycle stability and high capacitance retention. Ti^{4+} does not have electrochemical activity, and the chemical valence does not change before and after charge and discharge. The discharge capacity of Ti^{4+} substituted cathode materials is slightly attenuated compared with that of unsubstituted cathode materials, but the stability is improved. Surprisingly, the materials kept their tunneling structure when the sodium content was raised [96].

Replacing the double ions with the cationic manganese with iron and titanium provided a stable cathode material $Na_{0.61}Mn_{0.27}Fe_{0.34}Ti_{0.39}O_2$, which was synthetically prepared in a solid-state using additional dopant precursors of Fe_2O_3 and anatase TiO_2 [43]. Its higher usable capacity is about 90 mAh/g, and its performance was outstanding in all tunneling cathode materials. Fe^{3+} is an electrochemical active ion and participates in redox reaction during charge and discharge, which is beneficial to increase discharge capacity. When hard carbon was used as the anode electrode, the reversible capacity and cycling performance of the rechargeable battery are very excellent, and the discharge capacity can reach 300 mAh/g. This new electrode material has great potential to be a candidate for large-scale application. The synthetic route of the material is simple, and the function is rich. Not only can it be used as cathode material, but also can be extended to the anode material, to guide the development direction of new materials.

The crystal structure of $NaAl_{0.1}Mn_{0.9}O_2$ is changed from pure tunnel-type to hybrid layered structure after the doping of Al ions at the sodium site. The replacement material has high stability of the cathode material due to the formation of Al-O bonds on the surface of the material. The replacement of aluminum has high stability due to forming shape of a very stable Al-O bond on the surface [42]. Although the introduction of aluminum can cause phase transition, it can improve the stability of particles. The surface stability of particles is better because of the formation of Al-O bonds than that of tunnel-type NMO. $NaAl_{0.1}Mn_{0.9}O_2$ showed a high discharge capacity. The initial discharge capacity was 145 mAh/g, and the capacity retention rate was 71.0% after 100 cycles. Compared with NMO, the capacity retention rate was higher. The high initial discharge capacity of the cathode material is the formation of the orthogonal laminated $NaMnO_2$ phase.

The performance of zirconium doped $Na_{0.44}Mn_{1-x}Zr_xO_2$ cathode material is brilliant [97]. *In situ* X-ray diffraction shows that the volume change of $Na_{0.44}Mn_{0.98}Zr_{0.02}O_2$ optimized by Zr doping is less than 5% during the initial charge-discharge process. In addition, the diffusion coefficient of Na^+ is significantly increased, and the multiplier performance is significantly improved. A high reversible capacity of 112 mAh/g can be obtained at 1 C. The 78 mAh/g can be maintained after 1000 cycles and retains 80% capacity at 5 C to support a long cycle life. It shows that Zr substitution provides a new idea for optimizing excellent performance cathode of sodium-ion battery.

NMO nanorods substituted by B can be synthesized by solid-phase method [98]. As the content of B increases, the appearance of the impurity phase can be seen in the XRD of $NaMn_{2-x}B_xO_4$. The temperature of α-Mn_2O_3 is higher than that of another manganese alloy [41,99]. It is shown that the contents of α-Mn_2O_3 and $Na(BO_2)_2$ sections increase with the decomposition of the NMO phase. The content of boron is reciprocally proportional to the number of nanorods. The number of nanorods is inversely proportional to the amount of boron content. When the boron content increases, the number of nanorods decreases in a particular proportion, and the particle size and strain will decrease accordingly. Because the B ion may be immersed in the NMO phase, the *C* axis will increase monotonically. At the same time, the increase of boron content will produce the boron impurity phase. By affecting the growth of nanotubes, the morphology of nanorods is concerned, and the surface area is increased, and the length is decreased, which is anticipated to be employed in reversible sodium-ion batteries.

Lithium exchange has been attempted at sodium sites [90]. Some dopants such as cobalt led to phase transformation from the original tunnel-type structure towards the P2-type layer structure [100]. $Na_{0.44}Mn_{0.89}Co_{0.11}O_2$ substituted with cobalt offers greater discharge capacity with excellent retention capacity [101].

Fluoride doping at oxygen sites can reduce the bond energy between oxygen atoms and enhance the diffusion of Na^+. $Na_{0.44}MnO_{1.93}F_{0.07}$ material can be synthesized by the sol-gel method, and the cathode material obtained has high discharge specific capacity and cycling performance [102]. The results show that fluorine substitution may be an effective method to change NMO tunnel-type structure and enhanced electrochemical activity. It also provides a high-level argument for superior performance composite structural cathodes for SIBs that introduce halogen anions to exchange structural oxygen.

The Mg^{2+} was introduced into the hinge of the cathode material of the Mn-based tunnel structure. The tunnel-type structure NMO promotes the transport of Na^+ and reduces the released energy of sodium. By adding electrons near the Fermi level, the stability of the front cycle and the performance of the various rate are enhanced to some extent, and highly reversible electrochemical reactions and phase transitions are realized in the cathode. The initial discharge capacity of $Na_{0.44}Mn_{0.95}Mg_{0.05}O_2$ remains 67% after 800 cycles at 2 C, which is significantly higher than that of without doped NMO [103]. This method can improve the properties of cathode materials for tunnel structures.

Although the doped crystal structure can improve the electrochemical performance to a certain extent, this modification method will change the pure tunnel-type structure into another phase. The electrochemical performance can also be enhanced by co-doping the two elements [104], which reports the substitution of manganese for Fe and Ti cathode materials. In addition, the co-doping elements are chromium and lithium, which can still form a tunnel structure. However, the structure of Al-doped Mn site is a mixed phase of layered and tunnel structure, and the substitution of cobalt and fluoride at Mn site will result in the transformation of crystal structure from tunnel structure to P2-type layered structure. Single cationic and cationic doping or co-doping can further study the doped ions and doping mechanism.

3.3. Surface coating on NMO

Another way to modify materials is to apply a coating to the surface of the material. The coated cathode material can form a protective layer on the surface of the cathode material, which acts as a buffer and can promote the diffusion of surface charge to avoid the occurrence of side reactions. Zhao *et al.* [36] coated NMO with a layer of Na_2MoO_4 by molten impregnation, which can promote electron transfer in SIBs. The surface layer of Na_2MoO_4 has a significant contribution to the stability of cathode materials in high-rate sodium storage. The coated material has improved capacity and high efficiency, and even at the rate of 60 C, it also has about 100% excellent performance until 1000 cycles. It was surprising that the NMO electrode has an amazing capacity retention of up to 1000 cycles at 60 °C. For 5–10 nm coating on the surface can show the excellent cycle performance of the electrode at high speed. The SEM comparison diagram at low magnification was not shown in this paper, and the influence of coating amount on par-

ticle agglomeration can be further explored, as shown in Fig. S3 (Supporting information).

Strikingly, 2 wt% $NaTi_2$ $(PO_4)_3$ coating NMO cathode materials synthesized by sol-gel method [67] or hydrothermal method [105] inhibits cationic dissolution [106]. $Na_2Ti_6O_{13}$ has high conductivity, this advantage can suppress the phase change process of the positive electrode material coated with this material and enhance the stability of the crystal structure as presented. As the pictures show, the cyclic voltammetry characteristic curves show six redox peaks. And there are two kinds of phase transitions in the whole process of charge and discharge. In agreement with the CV results, six voltage platforms conjointly appeared on the initial charge and discharge curves of the NMO and $NaTi_2(PO_4)_3$ (NTP) coated samples. The polarization of the NTP coated sample is slightly less than that of the original sample. For the cycling and rate properties, the coated sample was significantly improved.

The chemical stability will be affected in the high voltage region, and the chemical stability will be improved by Al_2O_3 coating on the cathode material surface [107]. The performance of the cathode material passed through the alumina layer is better than that of the original submicron rod NMO. Using Al_2O_3 as the layer can prevent the direct contact between the submicron rod and the electrolyte, and more importantly, it can prevent the volume expansion in the electrochemical process, which has certain reference significance for the surface coating. The direction of the research has always been to prepare materials with good stability and good diffusion kinetics.

4. Sodium ion battery applications

Among many tunnel structures, NMO is a typical hot spot and widely used in SIBs [108]. The diffusion of Na^+ in different positions will cause different redox peaks. It can be concluded that the peak current of cathode and anode in the nonaqueous electrolyte is larger than in the aqueous electrolyte, so the electrical conductivity and specific capacity in the nonaqueous electrolyte are higher than that in the aqueous electrolyte. Li *et al*. proved that the crystal structure is completely consistent with the tunnel structure by high angle annular dark field images. The electron energy loss spectrum can clearly distinguish the sodium and transition metal sites, and it can be inferred that the valence states of Mn and Ti are Mn^{3+} and Ti^{4+}, respectively. The Mn(3) site was filled with Ti ions, and the remaining Mn sites were filled with Mn ions, as shown in Fig. S4 (Supporting information). Aqueous based SIBs have received extensive and in-depth research in recent years due to their outstanding advantages such as high safety, low cost and environmental friendliness, and have made great progress while gradually starting the industrialization process. Due to its outstanding advantages of low cost, high safety, sustainability and environmental friendliness, water system SIBs have a broad application prospect in the field of large-scale stationary energy storage. Recently, some domestic and foreign research institutions and enterprises have increased investment and deepened the layout of practical water sodium-ion batteries. Aquion Energy is the first company to mass produce water sodium-ion batteries in the world. Using manganese oxide as the positive electrode, carbon as the negative material, and Na_2SO_4 aqueous solution as the electrolyte, they assembled a battery with good test results, which can continue to charge and discharge more than 5000 times, and has an efficiency of more than 85%, at less than one third of the cost of lithium-ion batteries. The number of domestic ion battery production lines have been built and put into operation since 2015, and the demonstration in the field of energy storage has been realized. At present, researchers have done very detailed and in-depth research on the electrode materials and electrolyte of water sodium ion battery, and its cycle life and multiplier performance have reached a higher degree. However, the thermodynamic decomposition voltage of water is only 1.23 V, which greatly limits the operating voltage and energy density of the water sodium ion battery. This leads to a lot of water sodium ion battery anode materials cannot be used in practice. To solve these problems, researchers have made a lot of active exploration in the development and modification of electrode materials and electrolyte. However, compared with organic secondary batteries, aqueous-based SIBs are still greatly limited by the narrow electrochemical stability window of the electrolyte and the poor cyclic stability of the electrode materials. So far, how to solve these problems remains the key to the development of this field.

4.1. Neutral electrolyte

Whitacre reported that $Na_4Mn_9O_{18}$ was used as a cathode material for SIBs for aqueous-electrolyte energy storage devices, The specific capacity of $Na_4Mn_9O_{18}$ in the neutral electrolyte was 45 mAh/g by solid-state reaction [109,110]. When the mass ratio of positive and anode electrodes is adjusted, the battery can be charged to about 1.7 V with no significant hydroelectric solution. Li *et al*. [111] study demonstrated that the whole battery in $NaTi_2(PO_4)_3$/NMO aqueous solution exhibited ultra-fast rate capability and excellent high-rate cycling stability, which was the higher specific capacity of sodium electric system reported so far in the sodium ion aqueous solution system [111]. At a current of up to 90 C (144 mA/cm^2), the reversible capacity of the entire cell is 70% of that of 3 C, and the capacity retention rate was about 60% after 700 cycles. Wang *et al*. [37] prepared a new type of sodium rich tunnel-type cathode material by solid phase method, which was Ti-substituted $Na_{0.66}Mn_{0.66}Ti_{0.34}O_2$. Using $NaTi(PO_4)_3$/C as the anode material, $NaTi(PO_4)_3$/C showed a high specific capacity of 76 mAh/g in 1 mol/L $NaSO_4$ aqueous electrolyte at a current of 2 C.

4.2. Alkaline electrolyte

Although NMO exhibited good cyclic stability in neutral electrolyte, the previously reported discharge capacity only was 40 mAh/g, which was mainly because H^+ in water limited the intercalation/deintercalation of Na^+. The advantage of using alkaline electrolyte is that the activity of H^+ can be reduced, so that the H^+ intercalation is affected. The electrochemical properties of NMO in alkaline electrolyte were reported for the first time by Yuan *et al*. [112]. In the voltage range of 1.95–1.1 V, the reversible capacity of 6 mol/L NaOH electrolyte was 80.2 mAh/g, superior to neutral electrolyte. At the current rate of 20 C, the reversible capacity of the NMO electrode is showing excellent rate performance around 42.7 mAh/g. They also found that the NMO electrode was highly resistant to overcharging, which not only has good rate performance and cycling performance in alkaline electrolyte, but NMO-base alkaline battery also has the advantages of metal corrosion resistance. Increasing the NaOH concentration is beneficial to inhibit the occurrence of hydrogen intercalation reaction and improve the cycle performance and rate performance of the electrode, but at the same time it will also cause the early triggering of the oxygen evolution reaction. If the concentration is too high, the rate performance will be reduced. In addition, we can reduce the side reaction and improve the cycle performance by reducing the voltage window. NMO also shows excellent overcharge resistance in concentrated alkaline electrolyte. This not only indicates that the sodium storage performance of NMO can be greatly improved by optimizing the electrolyte system and test conditions, but also indicates that NMO as the cathode material of aqueous SIBs has a good application prospect in the field of large-scale energy storage.

4.3. Ionic liquid electrolyte media

SIBs can also use ionic liquid electrolytes [113]. Butylmethylpyridine-bis (trifluoromethonyl) imide (BP-TFSI) ionic liquid (IL) or glycine [70] with various sodium solute, namely $NaBF_4$, $NaClO_4$, NaTFSi and $NaPF_6$, acts as electrolytes for rechargeable Na/NMO batteries. Because in the ionic electrolyte, the electrolyte has high stability can be used at high temperature. In the electrolyte containing $NaClO_4$, the electrode material showed good electrochemical performance. When the charge and discharge ratio is increased to 1 C, the capacity retention rate is 85%. With 1 mol/L $NaNO_3$ and 0.96 mol/L $Mn(NO_3)_2$ added to solid glycine as the electrolyte, the cyclic voltammetry characteristic curves of NMO cathode material were tested in the scanning frequency range of 20–400 mV/s. The current density of $Na_{0.7}MnO_{2.05}$ synthesized at 850 °C is proportional to the scan rate. Reaction situation is the same as that of reaction a, and the current density of NMO synthesized at 900 °C is also proportional, the rate of increase is significantly faster. In summary, it is shown that the cyclic reversibility of Na^+ is relatively stable and does not change with the change of charge and discharge rate. The performance of this electrolyte is better than that of a traditional electrolyte.

5. Challenges and future outlook

Reversible SIBs as a feasible specific application different from lithium-ion battery technology has attracted great attention of scientific researchers, and a large amount of energy storage will be considered as the most important use of secondary sodium-ion battery. Energy density, cost analysis, cycle stability, safety and ion diffusion rate are still the five main problems faced by SIBs. The advantages of SIBs are their high energy density and the ability to store large amounts of energy. Various cathode materials have been reported, including manganese oxides, sulfides, fluorides, polyanionic compounds, and metal-organic frameworks. Among them, tunnel-type transition metal oxide cathode materials have attracted attention due to their abundant cost and content. This article reviews many artificial techniques for preparing NMO, especially solid phase transition, molten salt, co-precipitation and inverse microemulsion. In an aqueous electrolyte system, the Mn-based tunnel transition metal oxide electrode exhibits a good rate capacity, but a hydrolysis reaction may occur. The electrochemical performance can be improved by cation substitution and surface coating. The size and structure of dopant atoms will not change due to cation substitution. There are many phase transitions and structural changes during the electrochemical reaction, and the cycle life of oxide materials is limited; polyanionic materials have longer cycle life and higher cycle life due to their stable structure. However, the larger anionic group limits the energy density of the material to a certain extent; the Prussian blue compound has a higher energy density, and it is the key to find a suitable synthesis method to obtain a higher purity material. In addition, amorphous materials with weak lattice limit have great research prospects, but they face the following three difficulties: (1) The low conductivity of the material is not conducive to the high rate performance of the battery, so the conductivity of the material will be reduced. Heat treatment, ion doping, carbon coating and other means to improve electrochemical performance; (2) Poor chemical stability and acid and alkali resistance, active materials may be dissolved in the electrolyte, poor cycle performance, can change the composition of amorphous materials, Adjust the physical and chemical properties of materials to achieve a balance between physical and chemical properties and electrochemical properties; (3) There is no clear theory on the structural changes of amorphous materials during charge and discharge, which is not conducive to improving the electrochemical properties of glass materials, and further research is needed. At present, the development of high-energy-density water-based sodium-ion batteries mainly faces the following challenges: (1) Electrode materials are generally nanomaterials, and it is difficult to achieve high loads. Even after a high load, the contact area between the electrode active material and the electrolyte increases. In addition, more interface side reactions (such as electrolyte decomposition, catalytic reactions) will be triggered. However, if micron-level electrode materials (such as micron-level Prussian blue analogs and NTP) are used directly, the electronic and ion conductance will be significantly reduced, resulting in a decrease in specific capacity, thereby affecting the density of energy batteries. (2) Due to the many side reactions of water-based electrolytes, the currently reported coulombic efficiency of water-based sodium-ion batteries are generally lower than 99.5%, so water-based batteries usually require a large amount of electrolyte to maintain relatively good cycle stability. However, the increase in the amount of electrolyte is bound to improve the quality of the entire battery. Therefore, the energy density of the device is reduced. The use of high-concentration electrolyte can effectively broaden the electrochemical stability window and increase the energy density to a certain extent, but at the same time it will increase the cost and reduce the economic benefit. In addition, some high-concentration electrolytes may also be toxic, which may cause some unavoidable environmental problems. Therefore, it is necessary to continue to develop low-cost and environmentally friendly methods to broaden the electrochemical stability window of the aqueous system electrolyte. In order to achieve large-scale production of NMO, the solid-state method can be considered. Sodium and manganese sources were uniformly mixed according to a certain stoichiometric ratio, and the mixture was subjected to chemical reaction at high temperature. Solid phase method has the advantages of low cost, simple synthesis process, less pollution, avoiding or reducing agglomeration in liquid phase reaction. It is a method that can realize large-scale production. In short, in the past five years, the research on sodium storage cathode materials has attracted much attention, and new structures and new systems have emerged one after another, which will greatly promote the application and development of SIBs.

Declaration of competing interest

The authors declare that they have no known competing financial interests or personal relationships that could have appeared to influence the work reported in this paper.

Acknowledgments

This work was supported by the National Natural Science Foundation of China (NSFC, Nos. 51804035, 51874079 and 51674068, the Hebei Province Key Research and Development Plan Project (No.19211302D). The authors wound also like to thank the support from Natural Science Foundation of Hebei Province (No. E2018501091), The Fundamental Research Funds for the Central Universities (Nos. N172302001, N182306001, N182312007, N2023040). The authors would also like to thank the support from Research Project on the Distribution of Heavy Metals in Soil and Comprehensive Utilization Technology of Tailings in Typical Iron Tailing Reservoir Areas of Hebei Province (No. 802060671901).

Supplementary materials

Supplementary material associated with this article can be found, in the online version, at doi:10.1016/j.cclet.2021.09.077.

References

[1] Y. Song, X. Li, C. He, et al., Chin. Chem. Lett. 32 (2020) 1106–1110.

[2] J. Heo, M. Chae, J. Hyoung, et al., Inorg. Chem. 58 (2019) 3065–3072.
[3] M. Chae, J. Heo, J. Hyoung, et al., ChemNanoMat 6 (2020) 1049–1053.
[4] D. Aurbach, Z. Lu, A. Schechter, et al., Nature 407 (2000) 724–727.
[5] M. Chae, J. Heo, H. Kwak, et al., J. Power Sources 337 (2017) 204–211.
[6] S. Kim, D. Seo, X. Ma, et al., Adv. Energy Mater. 2 (2012) 710–721.
[7] M. Slater, D. Kim, E. Lee, et al., Adv. Funct. Mater. 23 (2013) 947–958.
[8] L. Wang, Y. Lu, J. Liu, et al., Angew. Chem. Int. Ed. 52 (2013) 1964–1967.
[9] L. Yang, S. Luo, Y. Wang, et al., Chem. Eng. J. 404 (2021) 126578.
[10] S. Komaba, C. Takei, T. Nakayama, et al., Electrochem. Commun. 12 (2010) 355–358.
[11] H. Xu, C. Cheng, S.Y. Chu, et al., Adv. Funct. Mater. 30 (2020) 2005164.
[12] Q. Li, S. Xu, S.H. Guo, et al., Adv. Mater. 32 (2020) 1907936.
[13] H. Ren, Y. Bai, X.R. Wang, et al., ACS Appl. Mater. Interface 11 (2019) 37812–37821.
[14] C. Pu, J. Yu, L. Fu, et al., Chin. Chem. Lett. 32 (2020) 1081–1085.
[15] T. Jin, H. Li, K.J. Zhu, et al., Chem. Soc. Rev. 49 (2020) 2342–2377.
[16] M. Doeff, T. Richardson, L. Kepley, et al., J. Electrochem. Soc. 143 (1996) 2507–2516.
[17] M. Chae, Y. Elias, D. Aurbach, et al., ChemElectroChem 8 (2021) 798–811.
[18] J. Parant, R. Olazcuaga, M. Devalette, et al., J. Solid State Chem. 3 (1971) 1–11.
[19] A. Mendiboure, C. Delmas, P. Hagenmuller, et al., J. Solid State Chem. 57 (1985) 323–331.
[20] M. Doeff, M. Peng, Y. Ma, et al., J. Electrochem. Soc. 26 (1994) 141–145.
[21] Y. Li, Y. Xu, Z. Wang, et al., Adv. Energy Mater. 8 (2018) 1800927.
[22] D. Zhou, C. Lib, F. Yina, et al., Chin. Chem. Lett. 31 (2020) 2325–2329.
[23] J. Liang, L. Zhang, D. Li, et al., Rare Metals 39 (2020) 1005–1018.
[24] Y. Yang, W.F. Wei, et al., Rare Metals 39 (2020) 332–334.
[25] J. Akimoto, H. Hayakawa, N. Kijima, et al., Solid State Phenomen. 170 (2011) 198–202.
[26] F. Sauvage, E. Baudrin, J.M.J.S. Tarascon, et al., Sens. Actuator B: Chem. 120 (2007) 638–644.
[27] F. Sauvage, L. Laffont, J.M. Tarascon, et al., Inorg. Chem. 46 (2007) 3289–3294.
[28] L. Yang, Shaohua Luo, Y. Wang, et al., Chin. Chem. Lett. 31 (2020) 3200–3204.
[29] M. Chae, H. Kim, J. Lyoo, et al., Adv. Energy Mater. 10 (2020) 2002205.
[30] I. Kruk, P. Zajdel, W. Beek, et al., J. Am. Chem. Soc. 133 (2011) 13950–13956.
[31] Y. Liu, T. Zhou, Y. Zheng, et al., ACS Nano 11 (2017) 8519–8526.
[32] J. Wu, Z. Shen, W. Yang, et al., Front. Chem. 8 (2020) 816.
[33] R. Qiao, K. Dai, J. Mao, et al., Nano Energy 16 (2015) 186–195.
[34] F. Gu, T. Sun, X. Yao, et al., J. Phys. Chem. Solids 149 (2021) 109771.
[35] H. Ma, H. Su, K. Amine, et al., Nano Energy 43 (2018) 1–10.
[36] C. Zhao, Q. Wang, Z. Yao, et al., Science 370 (2020) 708–711.
[37] Y. Wang, L.Q. Mu, J. Liu, et al., Adv. Energy Mater. 5 (2015) 1501005.
[38] P. Zhan, K.L. Jiao, J.X. Wang, et al., J. Electrochem. Soc. 162 (2015) A2296–A2301.
[39] D. Zhang, W.J. Shi, Y.W. Yan, et al., Electrochim. Acta 258 (2017) 1035–1043.
[40] Z.X. Chen, T.C. Yuan, X.J. Pu, et al., ACS Appl. Mater. Interface 10 (2018) 11689–11698.
[41] G.Y. Ma, Y. Zhao, K.S. Huang, et al., Electrochim. Acta 222 (2016) 36–43.
[42] D.W. Han, J.H. Ku, R.H. Kim, et al., ChemSusChem 7 (2014) 1870–1875.
[43] S. Xu, Y. Wang, L. Ben, et al., Adv. Energy Mater. 5 (2015) 1501156.
[44] L. Zhao, J. Ni, H. Wang, et al., RSC Adv. 3 (2013) 6650–6655.
[45] Y. Zhang, L. Liu, S. Jamil, et al., Appl. Surf. Sci. 494 (2019) 1156–1165.
[46] X. Ju, H. Huang, H. Zheng, et al., J. Power Sources 395 (2018) 395–402.
[47] Jiangying Yu, Hong, et al., Mater. Lett. 164 (2016) 440–443.
[48] L. Zhao, J. Ni, H. Wang, et al., Funct. Mater. Lett. 6 (2013) 50012.
[49] X.L. Jiang, S. Liu, H.Y. Xu, et al., Chem. Commun. 51 (2015) 8480–8483.
[50] C. Liu, W.L. Guo, Q.H. Wang, et al., J. Alloy Compd. 658 (2016) 588–594.
[51] S.I. Hirano, R. Narita, S. Naka, et al., J. Cryst. Growth 54 (1981) 595–599.
[52] E. Hosono, T. Kudo, I. Honma, et al., Nano Lett. 9 (2009) 1045–1051.
[53] E. Hosono, T. Saito, J. Hoshino, et al., J. Power Sources 217 (2012) 43–46.
[54] Q. Feng, T. Horiuchi, L.H. Liu, et al., Chem. Lett. 3 (2000) 284–285.
[55] P. Zheng, J.X. Su, Y.B. Wang, et al., ChemSusChem 13 (2020) 1793–1799.
[56] X. Zhou, R.K. Guduru, P. Mohanty, et al., J. Mater. Chem. A (1) (2013) 2757–2761.
[57] Y. Zhang, Y. Ouyang, L. Liu, et al., J. Cent. South Univ. 26 (2019) 1510–1520.
[58] Y. Zhang, Z.X. Liu, H.Q. Deng, et al., ChemElectroChem 6 (2019) 1711–1721.
[59] K.Y. Shen, M. Lengyel, L. Wang, et al., MRS Commun. 7 (2017) 74–77.
[60] Y. Cao, L. Xiao, W. Wang, et al., Adv. Mater. 23 (2011) 3155–3160.
[61] B. Fu, X. Zhou, Y. Wang, et al., J. Power Sources 310 (2016) 102–108.
[62] Y. Liu, X. Liu, F. Bu, et al., Electrochim. Acta 313 (2019) 122–130.
[63] K.H. Dai, J. Mao, X.Y. Song, et al., J. Power Sources 285 (2015) 161–168.
[64] P. Zhan, S. Wang, Y. Yuan, et al., J. Electrochem. Soc. 162 (2015) A1028–A1032.
[65] Q.N. Liu, Z. Hu, M.Z. Chen, et al., ACS Appl. Mater. Interface 9 (2017) 3644–3652.
[66] Y. Xiao, P. Wang, Y. Yin, et al., Adv. Energy Mater. 8 (2018) 1800492.
[67] Y.H. Liu, D. Wang, J. Liu, et al., J. Alloy Compd. 849 (2020) 1501156.
[68] K. Liu, S.S. Tan, J. Moon, et al., Adv. Energy Mater. 10 (2020) 2000135.
[69] Z.W. Zhou, Z.Y. Luo, Z.J. He, et al., J. Power Sources 479 (2020) 228788.
[70] L. Rakocevic, S. Strbac, J. Potocnik, et al., Ceram. Int. 47 (2021) 4595–4603.
[71] G.S. Shinde, P.D. Nayak, S.P. Vanam, et al., J. Power Sources 416 (2019) 50–55.
[72] J.R. Wang, Q. Zhou, J.Y. Liao, et al., ACS Appl. Energy Mater. 2 (2019) 7497–7503.
[73] T. Tan, X. Tan, W. Wang, et al., ChemElectroChem 7 (2020) 2020–2025.
[74] L.F. Xiao, Y.Y. Yang, Y.Q. Zhao, et al., J. Solid State Electrochem. 12 (2008) 149–153.
[75] X. Zhou, Y. Lai, X. Wu, et al., Chem. Res. Chin. Univ. 37 (2021) 274–279.
[76] M. Okubo, E. Hosono, T. Kudo, et al., Solid State Ion. 180 (2009) 612–615.
[77] T. Kawamura, M. Makidera, S. Okada, et al., J. Power Sources 146 (2005) 27–32.
[78] M. Okubo, J. Kim, T. Kudo, et al., J. Phys. Chem. C 113 (2009) 15337–15342.
[79] H.B. Ren, Y.R. Wang, D.C. Li, et al., J. Power Sources 178 (2008) 439–444.
[80] J.W. Fergus, J. Power Sources 195 (2010) 939–954.
[81] S. Demirel, E. Oz, E. Altin, et al., Mater. Charact. 105 (2015) 104–112.
[82] D.W. Su, C.Y. Wang, H.J. Ahn, et al., Chem. Eur. J. 19 (2013) 10884–10889.
[83] Y.H. Liu, T. Takasaki, K. Nishimura, et al., J. Electrochem. Soc. 161 (2014) A1194–A1199.
[84] T.A. Tan, D.T. Phuong, N. Oanh, et al., Commun. Phys. 24 (2014) 233–238.
[85] Y.G. Li, Y.Y. Wu, et al., Nano Res. 2 (2009) 54–60.
[86] N. Sheng, C.G. Han, Y.H. Lei, et al., Electrochim. Acta 283 (2018) 1560–1567.
[87] X. He, J. Wang, B. Qiu, et al., Nano Energy 27 (2016) 602–610.
[88] D. Zhang, W.J. Shi, et al., Electrochim. Acta 258 (2017) 1035–1043.
[89] C. Ferrara, C. Tealdi, Asta V, et al., Batteries 4 (2018) 8.
[90] J. Akimoto, H. Hayakawa, N. Ishida, et al., J. Power Sources 244 (2013) 382–388.
[91] M.W. Xu, Y.B. Niu, C.J. Chen, et al., RSC Adv. 4 (2014) 38140–38143.
[92] Y.L. Cao, L.F. Xiao, W. Wang, et al., Adv. Mater. 23 (2011) 3155–3160.
[93] B. Fu, Y. Su, J.X. Yu, et al., Electrochim. Acta 303 (2019) 125–132.
[94] H. Kim, J. Hong, K.Y. Park, et al., Chem. Rev. 114 (2014) 11788–11827.
[95] N. Bucher, S. Hartung, I. Gocheva, et al., J. Solid State Electrochem. 17 (2013) 1923–1929.
[96] S.H. Guo, H.J. Yu, D.Q. Liu, et al., Chem. Commun. 50 (2014) 7998–8001.
[97] W.J Shi, X. Meng, et al., ChemElectroChem 7 (2020) 2545–2552.
[98] E. Oz, S. Demirel, S. Altin, et al., Ceram. Int. 42 (2016) 17059–17066.
[99] R.Y. Yue, F. Xia, R.J. Qi, et al., Chin. Chem. Lett. 32 (2021) 849–853.
[100] M.M. Doeff, T.J. Richardson, J. Hollingsworth, et al., J. Power Sources 112 (2002) 294–297.
[101] Y.T. Zhou, X. Sun, B.K. Zou, et al., Electrochim. Acta 213 (2016) 496–503.
[102] W.J. Shi, Y.W. Yan, C. Chi, et al., J. Power Sources 427 (2019) 129–137.
[103] X.L. Li, J. Bao, Y.F. Li, et al., Adv. Sci. 8 (2021) 2004448.
[104] S.Y. Xu, Y.S. Wang, L.B. Ben, et al., Adv. Energy Mater. 5 (2015) 1501156.
[105] L.Y. Liu, Y. Ding, B. Zhou, et al., Appl. Sci. Basel 9 (2019) 1673.
[106] Y. Zhang, L. Liu, S. Jamil, et al., Appl. Surf. Sci. 494 (2019) 1156–1165.
[107] J.U. Choi, J.H. Jo, C.H. Jo, et al., J. Mater. Chem. A 7 (2019) 13522–13530.
[108] D.J. Kim, R. Ponraj, A.G. Kannan, et al., J. Power Sources 244 (2013) 758–763.
[109] Z.S. Zhao, Y.H. Ye, W.H. Zhu, et al., Chin. Chem. Lett. 29 (2018) 629–632.
[110] X.K. Hou, W.H. Li, Y.Y. Wang, et al., Chin. Chem. Lett. 31 (2020) 2314–2318.
[111] Z. Li, D. Young, K. Xiang, et al., Adv. Energy Mater. 3 (2013) 290–294.
[112] Yuan T, Jiexin, et al., ACS Appl. Energy Mater. 10 (2018) 34108–34115.
[113] N. Zhu, K. Zhang, F. Wu, et al., Energy Mater. Adv. 2021 (2021) 9204217.